AIAA SciTech Forum
11–15 & 19–21 January 2021, VIRTUAL EVENT
AIAA Scitech 2021 Forum

10.2514/6.2021-1303

Study of Mach Number Effect on Cruise Efficiency for a Co-Flow Jet General Aviation Airplane

Yang Wang * Gecheng Zha †
Dept. of Mechanical and Aerospace Engineering
University of Miami, Coral Gables, Florida 33124
E-mail: gzha@miami.edu

Alexis Lefebvre ‡
Rand Simulation, an ANSYS Channel Partner

Abstract

This paper numerically studies the Mach number effect on cruise performance of a Co-Flow Jet (CFJ) general aviation (GA) airplane at freestream Mach number of 0.15, 0.30, and 0.46 with an aspect ratio of 21.3. An optimized CFJ-NACA-6421 airfoil is used for the CFJ wing. The advantages of using a thick airfoil are two folds: 1) higher cruise lift coefficient; 2) lighter weight. The numerical simulations employ the intensively validated in house FASIP CFD code, which utilizes a 3D RANS solver with Spalart-Allmaras (S-A) turbulence model, 3rd order WENO scheme for the inviscid fluxes, and 2nd order central differencing for the viscous terms. Two constant C_μ of 0.03 and 0.04 are studied to examine the effect on the aircraft cruise performance. The angle of attack (AoA) is held at 5° corresponding to the optimal aerodynamic and productivity efficiency in the previous study for the wing performance at different Mach number. At C_μ of 0.03, the flow is very well attached for Mach 0.15, which gives the highest pure lift to drag ratio C_L/C_D, the corrected aerodynamic efficiency with CFJ power coefficient included $(C_L/C_D)_c$, and the productivity efficiency $(C_L^2/C_D)_c$. When the Mach number is increased to 0.46, the lift coefficient is increased by 8.6% from 1.16 to 1.26 due to the compressibility effect, but all the three aerodynamic performance parameters, C_L/C_D, $(C_L/C_D)_c$, and $(C_L^2/C_D)_c$ drop substantially. The reason is that the a flow separation at the wing-fuselage junction occurs. The drag coefficient is significantly increased by 67% when the Mach number is increased form 0.15 to 0.46 due to the flow separation, higher skin friction drag, and higher induced drag. When the C_μ is increased to 0.04, the wing-fuselage junction flow separation is removed. The CFJ power coefficient is increased by 33%, but remains at a very low level due to the low energy expenditure feature of the CFJ flow control. The C_L/C_D, $(C_L/C_D)_c$, and $(C_L^2/C_D)_c$ are significantly increased by 21.3%, 10.7%, and 19.8% respectively. In other words, the CFJ power increased due to C_μ of 0.04 at Mach 0.46 is converted to more system efficiency gain reflected by enhanced $(C_L/C_D)_c$ and $(C_L^2/C_D)_c$, which include the CFJ power coefficient. The system efficiency gains are attributed to the increased C_L and substantially reduced C_D due to the removed flow separation at low CFJ energy expenditure.

Nomenclature

CFJ	Co-flow jet
AoA	Angle of attack

* Graduate Student
† Professor, AIAA associate Fellow
‡ Simulation Specialist, Ph.D.

LE	Leading Edge
TE	Trailing Edge
S	Planform area
c	Airfoil chord
U	Flow velocity
q	Dynamic pressure $0.5\,\rho\,U^2$
p	Static pressure
η	Pump efficiency
ρ	Air density
$\dot{m}$	Mass flow
M	Mach number
ω	Pitching Moment
P	Pumping power
∞	Free stream conditions
$_j$	Jet conditions
C_L	Lift coefficient $L/(q_\infty\,S)$
C_D	Drag coefficient $D/(q_\infty\,S)$
C_M	Moment coefficient
C_μ	Jet momentum coef. $\dot{m}_j\,U_j/(q_\infty\,S)$
$(C_L/C_D)_c$	CFJ airfoil corrected aerodynamic efficiency $L/(D+\,P/V_\infty)$
$(C_L^2/C_D)_c$	CFJ airfoil productivity efficiency $C_L^2/(C_D+\,P/V_\infty)$
Pc	Power coefficient $L/(q_\infty\,S\,V_\infty)$
PR	Total Pressure ratio of the CFJ pump
M_{is}	Isentropic Mach Number
M_∞	Freestream Mach Number
P_{tinj}	Total injection pressure
P_{tsuc}	Total suction pressure
V_{inj}/V_∞	Normalized injection velocity

1 Introduction

Using active flow control(AFC) to improve aircraft cruise efficiency is challenging because conventional aircraft usually are designed to have very high efficiency at cruise at low angle of attack with benign flow conditions. Active flow control provides promising avenues to break conventional aerodynamic limits and substantially enhance aircraft performance. Recently, the Co-Flow Jet (CFJ) flow control airfoil developed [1, 2, 3, 4, 5, 6, 7, 8, 9, 10, 11, 12] provides a promising concept to improve the cruise efficiency. In a CFJ airfoil, an injection slot near the leading edge (LE) and a suction slot near the trailing edge (TE) on the airfoil suction surface are created. As shown in Fig. 1, a small amount of mass flow is drawn into the suction duct, pressurized and energized by the micro compressor, and then injected near the LE tangentially to the main flow via an injection duct. The whole process does not add any mass flow to the system and hence is a zero-net-mass-flux(ZNMF) flow control. The CFJ airfoil is demonstrated to achieve radical lift augmentation, stall margin increase, drag reduction and increased nose-down moment for stationary and pitching airfoils. The CFJ airfoil has a unique low energy expenditure mechanism, because the jet gets injected at the leading edge peak suction location, where the main flow pressure is the lowest and makes it easy to inject the flow, and it gets sucked at the trailing edge, where the main flow pressure is the highest and makes it easy to draw the flow. The low energy expenditure is a key factor enabling

the CFJ airfoil to achieve high cruise efficiency [13] at low AoA when the flow is benign.

High cruise efficiency is particular important for electric aircraft due to the current low battery energy density. Lefebvre and Zha [13] conduct a conceptual aerodynamic design of an electric GA airplane using a CFJ-NACA-6421 airfoil. The airplane achieves excellent efficiency and range at Mach number 0.15. A thick airfoil with 21% thickness is rarely used for conventional aircraft design. The reason is that such a thick airfoil is prone to flow separation and stall. However, CFJ is advantages to remove flow separation and hence enables such a thick airfoil to be used. The advantages of using a thick airfoil are two folds: 1) higher cruise lift coefficient; 2) light weight.

The study for 3D wings at different Mach numbers conducted by Wang and Zha[14] indicates that the corrected aerodynamic efficiency with the CFJ power included drops significantly to the level of their baseline counterparts with no flow control. But the 3D CFJ wings significantly increase the cruise lift coefficient, net aerodynamic L/D, and the productivity efficiency of $C_L^2/(C_D)_c$.

Since AFC consumes external energy, it is essential to have low power consumption for the AFC at cruise. For an AFC driven by fluidic actuators, the AFC power consumption is linearly determined by the mass flow rate and exponentially determined by the total pressure ratio required by the actuators[15]. In other words, to reduce the AFC power consumption, it is desirable to increase the mass flow rate and reduce the total pressure ratio. Based on this guideline, Wang and Zha[16, 17, 18] further optimize the airfoil designed by Lefebvre and Zha [13] by enlarging the CFJ injection and suction slot size. Achieving the same lift coefficient, the CFJ power coefficient is significantly reduced. In particular, the CFJ airfoil with enlarged slot size can still achieve super-lift coefficient[17], but with substantially reduced power consumption. The optimized airfoil by Yang and Zha [16, 17, 18] is named CFJ6421-SST150-SUC247-INJ117 airfoil.

The previous design and study of the GA airplane is only at Mach number 0.15[13]. The purpose of this paper is to understand how the CFJ airplane performs at different Mach number, in particular with the optimized CFJ6421-SST150-SUC247-INJ117 airfoil. The results are important to provide information for a full CFJ vehicle for its aerodynamic performance and power requirement.

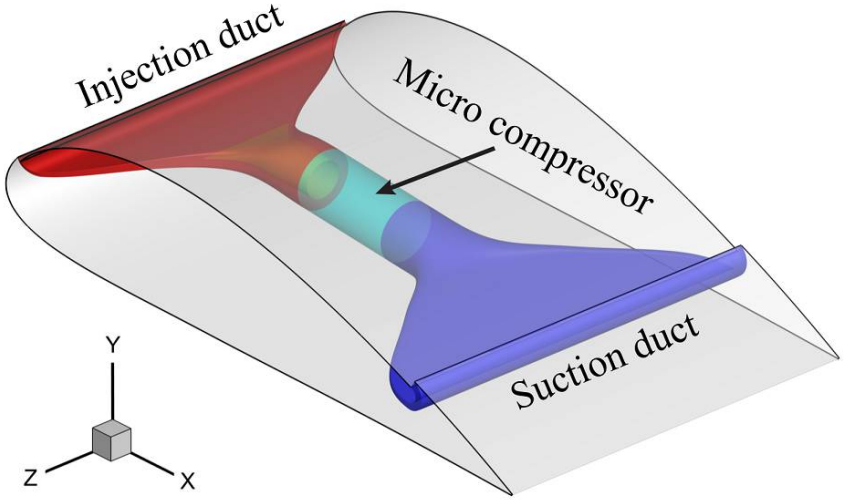

Figure 1: Schematic plot of a typical CFJ airfoil.

2 Co-Flow Jet Parameters

2.1 Lift and Drag Calculation

The momentum and pressure at the injection and suction slots produce a reactionary force, which is automatically measured by the force balance in wind tunnel testing. However, for CFD simulation, the full reactionary force needs to be included. Using control volume analysis as shown in Fig. 2, the reactionary force can be calculated using the flow parameters at the injection and suction slot opening surfaces. Zha et al. [2] give the following formulations to calculate the lift and drag due to the jet reactionary force for a CFJ airfoil. By considering the effects of injection and suction jets on the CFJ airfoil, the expressions for these reactionary forces are given as :

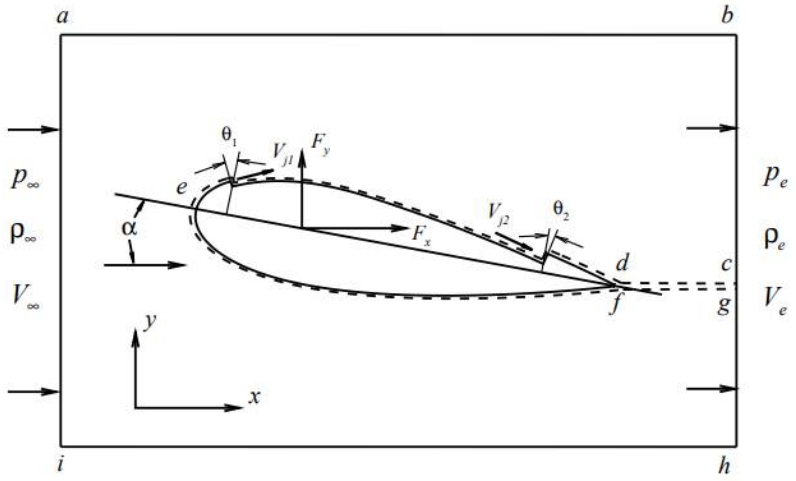

Figure 2: The control volume for a CFJ airfoil.

$$F_{x_{cfj}} = (\dot{m}_j V_{j1} + p_{j1} A_{j1}) * cos(\theta_1 - \alpha) - (\dot{m}_j V_{j2} + p_{j2} A_{j2}) * cos(\theta_2 + \alpha) \tag{1}$$

$$F_{y_{cfj}} = (\dot{m}_{j1} V_{j1} + p_{j1} A_{j1}) * sin(\theta_1 - \alpha) + (\dot{m}_{j2} V_{j2} + p_{j2} A_{j2}) * sin(\theta_2 + \alpha) \tag{2}$$

where the subscripts 1 and 2 stand for the injection and suction respectively, and θ_1 and θ_2 are the angles between the injection and suction slot's surface and a line normal to the airfoil chord. α is the angle of attack.

The total lift and drag on the airfoil can then be expressed as:

$$D = R'_x - F_{x_{cfj}} \tag{3}$$

$$L = R'_y - F_{y_{cfj}} \tag{4}$$

where R'_x and R'_y are the surface integral of pressure and shear stress in x (drag) and y (lift) direction excluding the internal ducts of injection and suction. For CFJ wing simulations, the total lift and drag are calculated by integrating Eq. (3) and Eq. (4) in the spanwise direction.

2.2 Jet Momentum Coefficient

The jet momentum coefficient C_μ is a parameter used to quantify the jet intensity. It is defined as:

$$C_\mu = \frac{\dot{m}V_j}{\frac{1}{2}\rho_\infty {V_\infty}^2 S} \tag{5}$$

where $\dot{m}$ is the injection mass flow, V_j is the mass-averaged injection velocity, ρ_∞ and V_∞ denote the free stream density and velocity, and S is the planform area.

2.3 Power Coefficient

CFJ is implemented by mounting a pumping system inside the wing that withdraws air from the suction slot and blows it into the injection slot. The power consumption is determined by the jet mass flow and total enthalpy change as the following:

$$P = \dot{m}(H_{t1} - H_{t2}) \tag{6}$$

where H_{t1} and H_{t2} are the mass-averaged total enthalpy in the injection cavity and suction cavity respectively, P is the Power required by the pump and $\dot{m}$ the jet mass flow rate. Introducing P_{t1} and P_{t2} the mass-averaged total pressure in the injection and suction cavity respectively, the pump efficiency η, and the total pressure ratio of the pump $\Gamma = \frac{P_{t1}}{P_{t2}}$, the power consumption is expressed as:

$$P = \frac{\dot{m}C_p T_{t2}}{\eta}(\Gamma^{\frac{\gamma-1}{\gamma}} - 1) \tag{7}$$

where γ is the specific heat ratio equal to 1.4 for air. The power coefficient is expressed as:

$$P_c = \frac{P}{\frac{1}{2}\rho_\infty V_\infty^3 S} \tag{8}$$

2.4 Corrected Aerodynamic Efficiency

The conventional wing aerodynamic efficiency is defined as:

$$\frac{L}{D} \tag{9}$$

For the CFJ wing, the ratio above still represents the pure aerodynamic relationship between lift and drag. However since CFJ active flow control consumes energy, the ratio above is modified to take into account the energy consumption of the pump. The formulation of the corrected aerodynamic efficiency for CFJ wings is:

$$(\frac{L}{D})_c = \frac{C_L}{C_D + P_c} \tag{10}$$

where V_∞ is the free stream velocity, P is the pumping power, and L and D are the lift and drag generated by the CFJ wing. The formulation above converts the power consumed by the CFJ into a force $\frac{P}{V_\infty}$ which is added to the aerodynamic drag D. If the pumping power is set to 0, this formulation returns to the aerodynamic efficiency of a conventional wing.

2.5 Aircraft Productivity

To compare aircraft that have the same ratio of initial weight to final weight with the same engine fuel consumption or battery energy density, the productivity efficiency C_L^2/C_D is introduced to measure the productivity of an airplane represented by its range multiplied by its weight [15].

The productivity efficiency $C_L^2/C_D = C_L(C_L/C_D)$ is a more comprehensive parameter than the conventional aerodynamic efficiency C_L/C_D to measure the merit of an airplane aerodynamic design for cruise performance. The former includes not only the information of C_L/C_D, but also the information of the aircraft weight C_L. For example, for two airplane designs having the same C_L/C_D with one C_L twice larger than the other, if the wing sizes are the same, one airplane will be able to carry twice more weight than the other with productivity and wing loading increased by 100%. Such a large difference is not reflected by C_L/C_D, but very well reflected by C_L^2/C_D.

The definition of C_L/C_D in general is a suitable measure of merit for conventional aircraft design. This is because at a certain Mach number regime, the maximum C_L/C_D is usually achieved at low angle of attack within the drag bucket and is more or less the same for different airfoil designs. In other words, for the same optimum C_L/C_D, the C_L is about the same. A typical C_L for subsonic airfoil is about 0.4 and for transonic airfoil is about 0.7.

For CFJ airfoil, the minimum CFJ pumping power occurs at a fairly high AoA [7, 19]. With the augmentation of CFJ, the subsonic cruise lift coefficient of a CFJ airfoil is typically 2 to 3 times higher than the conventional airfoil with about the same $(C_L/C_D)_c$ [12]. Such a high lift coefficient is unattainable for conventional airfoil since they would be either stalled or near stalled with very high drag. Hence for CFJ aircraft design, the productivity efficiency $C_L^2/C_D = C_L(C_L/C_D)$ is more informative to be used to reflect the aerodynamic performance. The corrected productivity efficiency for CFJ airfoils is $(C_L^2/C_D)_c = C_L^2/(C_D + P_c)$.

3 Numerical Algorithms

3.1 CFD Simulation Setup

The in house FASIP (Flow-Acoustics-Structure Interaction Package) CFD code is used to conduct the numerical simulation. The 3D Reynolds Averaged Navier-Stokes (RANS) equations with one-equation Spalart-Allmaras [20] turbulence model is used. A 3rd order WENO scheme for the inviscid flux [21, 22, 23, 24, 25, 26] and a 2nd order central differencing for the viscous terms [21, 25] are employed to discretize the Navier-Stokes equations. The low diffusion E-CUSP scheme used as the approximate Riemann solver suggested by Zha et al [22] is utilized with the WENO scheme to evaluate the inviscid fluxes. Implicit time marching method using Gauss-Seidel line relaxation is used to achieve a fast convergence rate [27]. Parallel computing is implemented to save wall clock simulation time [28].

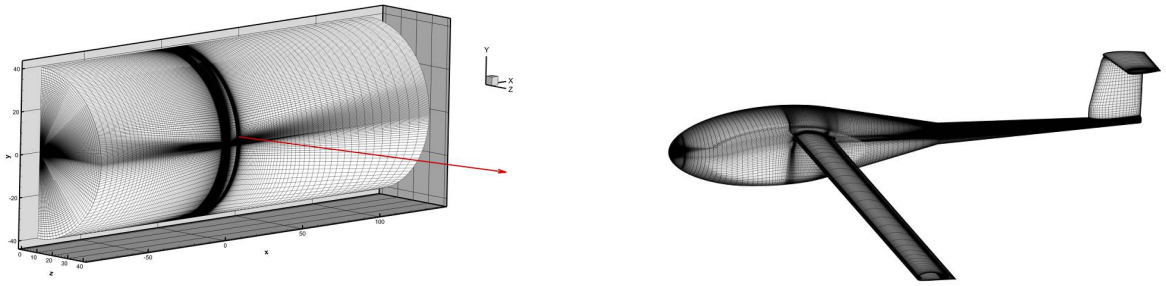

Figure 3: Computational mesh used in the current work.

3.2 Boundary Conditions

The 3rd order accuracy no slip condition is enforced on the solid surface with the wall treatment suggested in [29] to achieve the flux conservation on the wall. The computational mesh is shown in Fig. 3 with O-mesh topology and the radial farfield boundary located at 20 chord radius. The spanwise farfield is located at 20 chord away from the wing tip. The ducts geometries are predetermined based on our previous 2D designs [16]. Total pressure, total temperature and flow angles are specified at the injection duct inlet, as well as the upstream portion of the far field. Constant static pressure is applied at the suction duct outlet as well as the downstream portion of the far field. Symmetry boundary conditions are applied on the symmetric plane of the half airplane, whereas the wing tip flow is resolved by a mesh block. The mesh topology and size are the same as those used in [13] with total mesh size of 10.7 millions points split to 225 blocks for parallel computation.

4 Results and Discussion

4.1 CFJ Wing Geometry Parameters

The detailed parameters of CFJ airfoil used to create the 3D CFJ wing are presented by the injection and suction slot size normalized by airfoil chord length (C). The CFJ6421-SST150-SUC247-INJ117 airfoil designed in [16, 18] is optimized by enlarging the injection and suction size based on the CFJ airfoil from [12]. The CFJ6421-SST150-SUC247-INJ117 wing has a injection slot size of 1.17%C and suction slot size of 2.47%C. The suction surface translation (SST) is 1.50%C.

Table. 1 lists all the freestream conditions studied with the Mach number varying from 0.15 to 0.50 at the aspect ratio of 21.3. Since the focus is on the cruise performance, the AoA is fixed at 5° and the C_μ is studied at 0.03 and 0.04.

Table 1: Simulation cases

M_∞	AoA	C_μ	Re
0.15	5°	0.03, 0.04	1.34×10^6
0.30	5°	0.03, 0.04	2.67×10^6
0.46	5°	0.03, 0.04	4.10×10^6

4.2 Mach Contours and Isentropic Mach Number Plots

Fig. 4 shows the cross section Mach number contours along the wing span from root to the tip at different M_∞ and AoA of 5°, C_μ of 0.03. For Mach number 0.15, the CFJ momentum coefficient C_μ of 0.03 is sufficient to avoid any flow separation on the wing. But when the Mach number is increased to 0.3 and 0.46, a separation appears near the wing root at the conjunction of the wing and fuselage. Away from the wing root, the flow is clean all the way to the wing tip. When the C_μ is increased to 0.04 as shown in Fig. 5, the flow separation at the wing-fuselage is removed. An improved design could use a varying C_μ distribution with higher C_μ near the root and lower C_μ away from the root.

(a) M_∞= 0.15 C_μ = 0.03 (b) M_∞ = 0.30 C_μ = 0.03 (c) M_∞ = 0.46 C_μ = 0.03

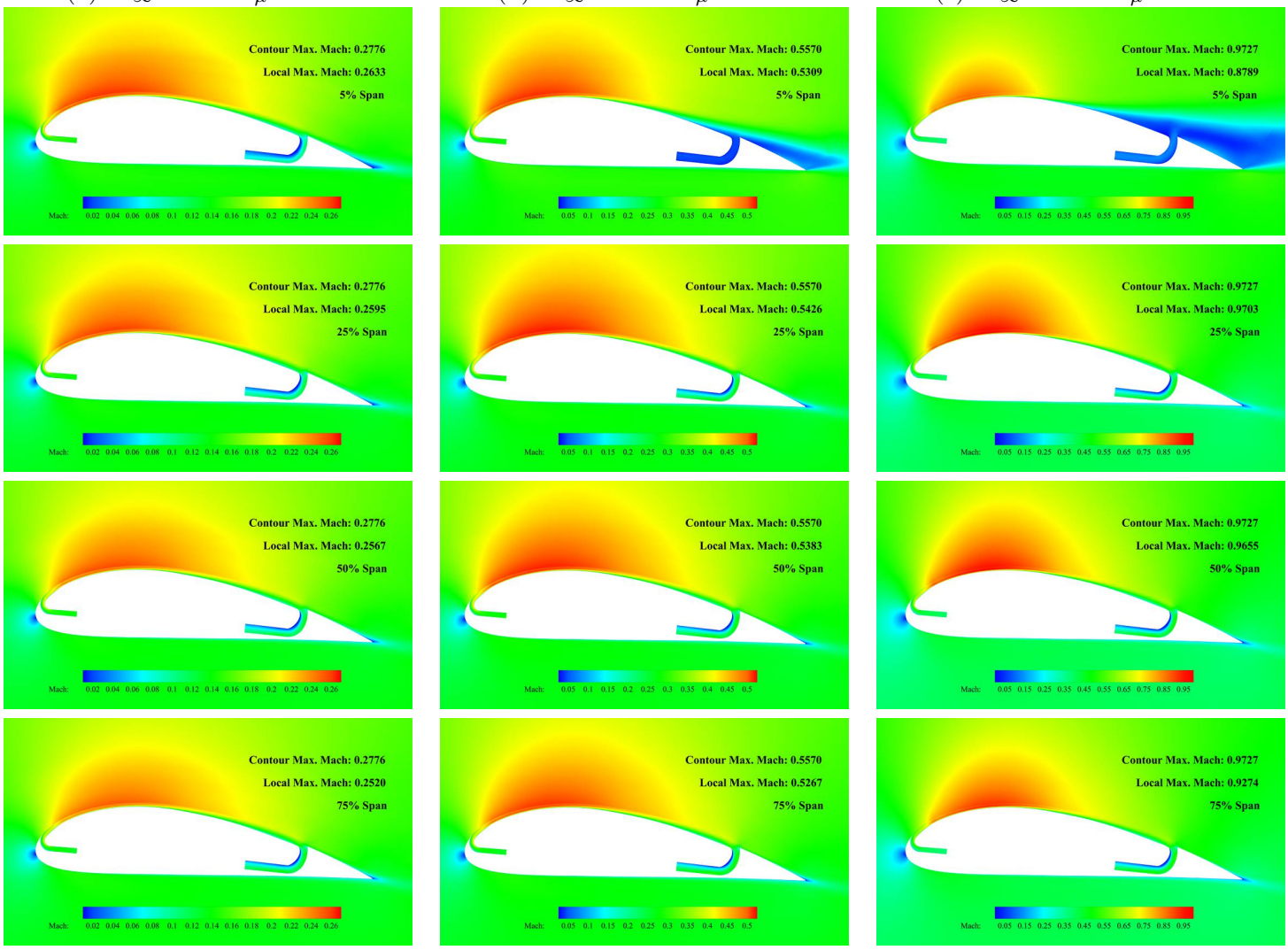

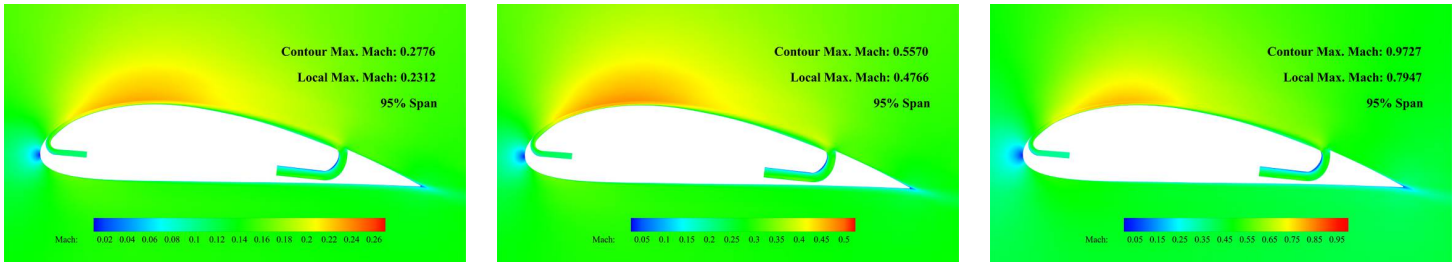

Figure 4: Mach contours at 5%, 25%, 50%, 75% and 95% spanwise location for the E-plane at different M_∞, $AoA = 5°$, $C_\mu = 0.03$.

(a) M_∞= 0.15 $C_\mu = 0.04$ (b) $M_\infty = 0.30$ $C_\mu = 0.04$ (c) $M_\infty = 0.46$ $C_\mu = 0.04$

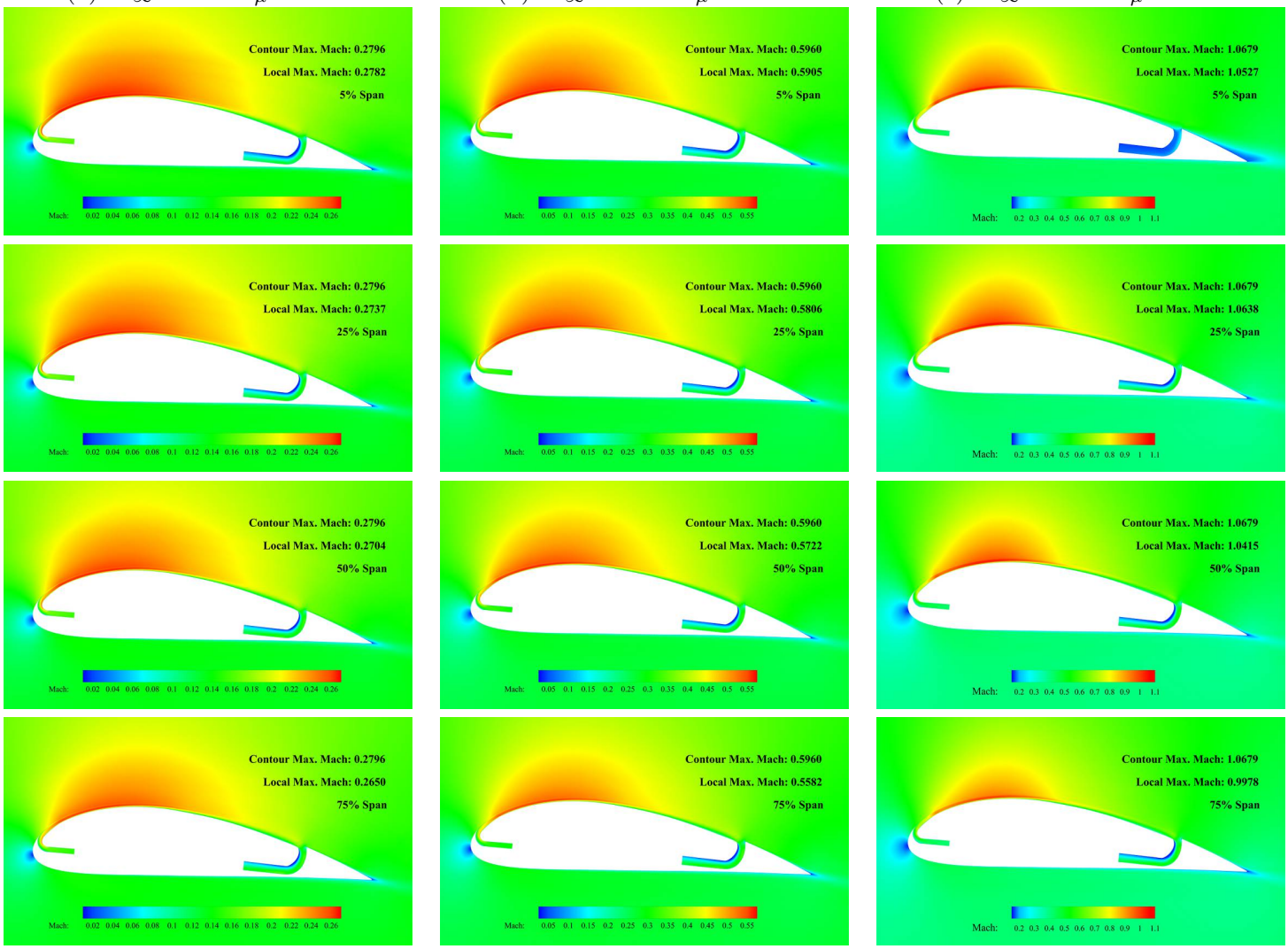

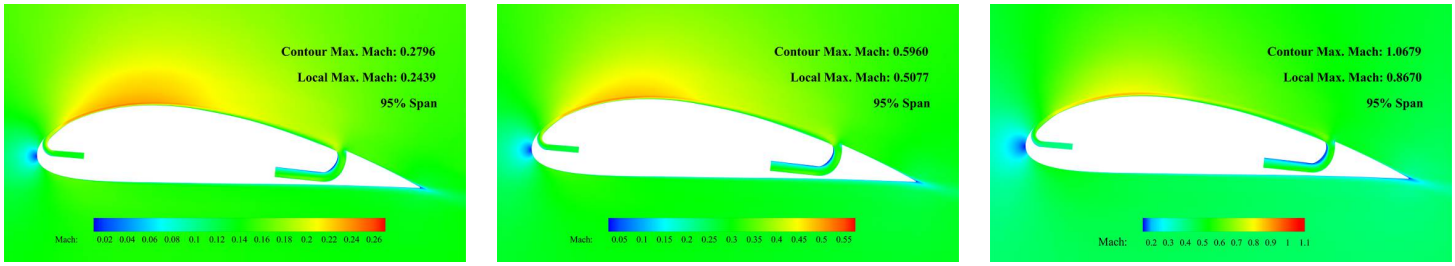

Figure 5: Mach contours at 5%, 25%, 50%, 75% and 95% spanwise location for the E-plane at different M_∞, $AoA = 5°$, $C_\mu = 0.04$.

Fig. 6 shows the airfoil surface isentropic Mach number along the wing span at different M_∞ and C_μ of 0.03 and 0.04, and AoA of 5°. Consistent with the Mach number contours plots along the span shown in Fig. 4 and Fig. 5, for C_μ of 0.03 at Mach number 0.15 and 0.3 (Fig. 6 (a) and (b)), the aerodynamic loading is fairly uniform from the wing root to the outer span until it is close to the tip, where the wing loading is decreased due to the tip vortex. For C_μ of 0.03 at the Mach number 0.46 (Fig. 6 (c)), the aerodynamic loading near the root is substantially deteriorated due to the flow separation at the corner of the wing and fuselage. When the C_μ is increased to 0.04 at Mach number 0.46 (Fig. 6 (f)), the wing root loading is restored due to the removal of the flow separation by the CFJ. Overall, the C_μ of 0.04 has higher aerodynamic load than C_μ of 0.03 as shown by the higher peak Mach number on the wing suction surface.

(a) M_∞= 0.15 C_μ = 0.03 (b) M_∞ = 0.30 C_μ = 0.03 (c) M_∞ = 0.46 C_μ = 0.03

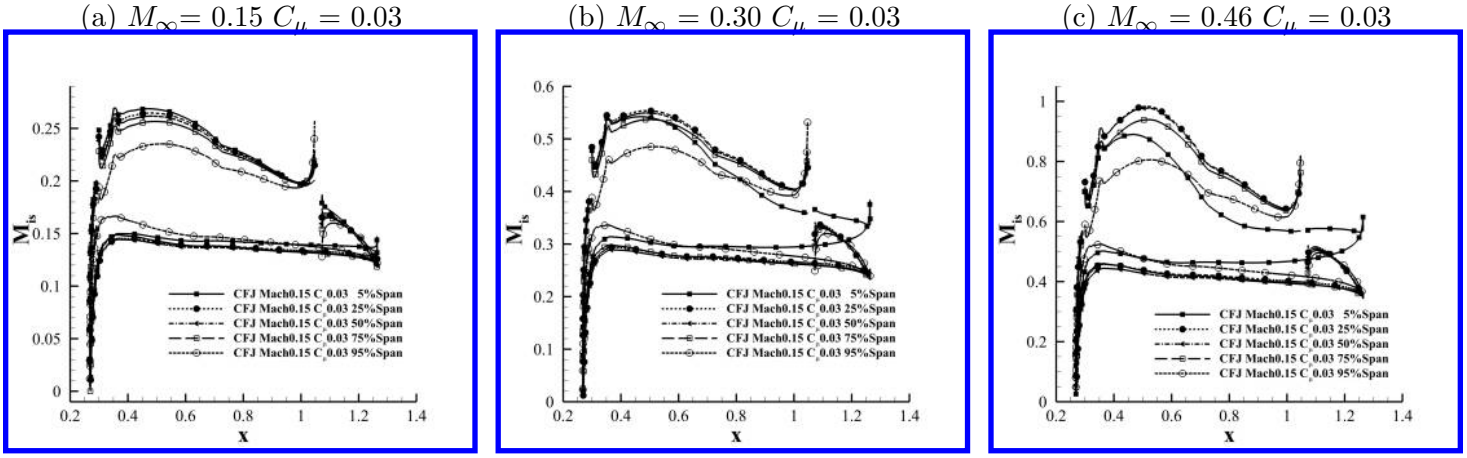

(d) M_∞= 0.15 C_μ = 0.04 (e) M_∞ = 0.30 C_μ = 0.04 (f) M_∞ = 0.46 C_μ = 0.04

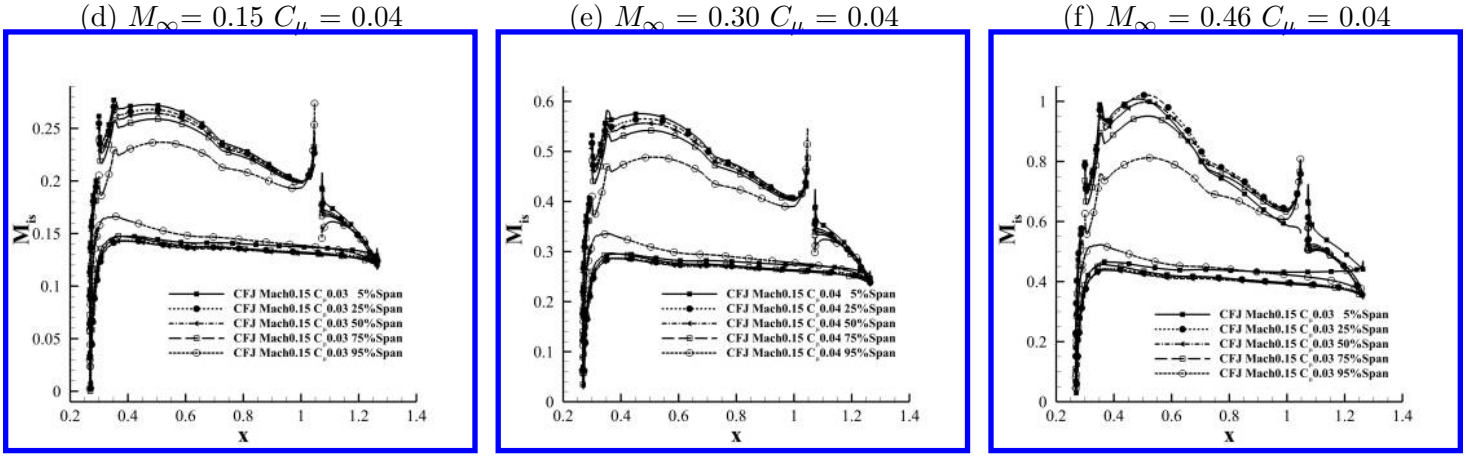

Figure 6: Isentropic Mach Number plots for the 3D CFJ airplane at different M_∞, C_μ of 0.03 & 0.04, and AoA of 5°.

In order to understand the force breakdown between the 3D CFJ wing and the fuselage, the lift and drag coefficient associated with the wing and fuselage are given in Table. 2. The drag of the fuselage is about 1/4 of the total drag and the wing has about 3/4 of the total drag for Mach number of 0.15 and 0.3. At Mach number 0.46, the wing drag percentage is slightly increased due to the flow is approaching supersonic on the suction surface.

Table 2: Force distribution at different M_∞ for the 3D airplane with CFJ Wing at AoA of 5° and C_μ of 0.03 & 0.04.

M_∞	AoA	C_μ	Parts	C_L	C_D
0.15	5°	0.03	Total	1.1597	0.0337
			Body	0.0994 (8.6%)	0.0083 (24.5%)
			Wing	1.0603 (91.4%)	0.0254 (75.5%)
0.15	5°	0.04	Total	1.2057	0.0338
			Body	0.1034 (8.6%)	0.0083 (24.7%)
			Wing	1.1023 (91.4%)	0.0254 (75.3%)
0.30	5°	0.03	Total	1.1685	0.0448
			Body	0.0639 (5.5%)	0.0102 (22.7%)
			Wing	1.1047 (94.5%)	0.0346 (77.3%)
0.30	5°	0.04	Total	1.2590	0.0418
			Body	0.0814 (6.5%)	0.0108 (25.8%)
			Wing	1.1776 (93.5%)	0.0310 (74.2%)
0.46	5°	0.03	Total	1.2603	0.0564
			Body	0.0628 (5.0%)	0.0117 (20.7%)
			Wing	1.1975 (95%)	0.0448 (79.3%)
0.46	5°	0.04	Total	1.3640	0.0504
			Body	0.0781 (5.7%)	0.0113 (22.4%)
			Wing	1.2859 (94.3%)	0.0391 (77.6%)

4.3 3D CFJ Airplane Performance at Different M_∞ and AoA

This section discusses the performance of 3D CFJ airplane at Different M_∞ and C_μ. With the Mach number increased from 0.15 to 0.46, the pure aerodynamic C_L/C_D and corrected $(C_L/C_D)_c$ are all decreased due to increased drag coefficient and CFJ power coefficient. At M_∞ of 0.46, the critical Mach number for the airfoil, the CFJ corrected aerodynamic efficiency is still very good since no shock appears in the flow filed.

As indicated by Table. 3, at C_μ of 0.03, the flow is very well attached for Mach 0.15, which gives the highest pure lift to drag ratio C_L/C_D, the corrected aerodynamic efficiency with CFJ power coefficient included $(C_L/C_D)_c$, and the productivity efficiency $(C_L^2/C_D)_c$. When the Mach number is increased to 0.46, the lift coefficient is increased by 8.6% from 1.16 to 1.26 due to the compressibility effect, but all the three aerodynamic performance parameters, C_L/C_D, $(C_L/C_D)_c$, and $(C_L^2/C_D)_c$ drop substantially. The reason is that a flow separation at the wing-fuselage junction occurs. The drag coefficient is significantly increased by 67% when the Mach number is increased from 0.15 to 0.46 due to the flow separation, higher skin friction drag, and higher induced drag. When the C_μ is increased to 0.04, the wing-fuselage junction flow separation is removed. The CFJ power coefficient is increased by 33%, but remains at a very low level due to the low energy expenditure feature of the CFJ flow control. The C_L/C_D, $(C_L/C_D)_c$, and $(C_L^2/C_D)_c$ are significantly increased by 21.3%, 10.7%, and 19.8% respectively. In other words, the CFJ power increased due to C_μ of 0.04 at Mach 0.46 is converted to more system efficiency gain reflected by enhanced $(C_L/C_D)_c$ and $(C_L^2/C_D)_c$, which include the CFJ power coefficient. The system efficiency gains are attributed to the increased C_L and substantially reduced C_D due to the removed flow separation at low CFJ energy expenditure.

Table 3: Performance at different M_∞ for the 3D airplane with CFJ Wing at AoA of 5° and C_μ of 0.03 and 0.04.

M_∞	AoA	C_μ	C_L	C_D	C_M	C_L/C_D	$(C_L/C_D)_c$	$(C_L{}^2/C_D)_c$	P_c
0.15	5°	0.03	1.1597	0.0337	0.0	34.4412	27.1488	31.4857	0.0090
0.15	5°	0.04	1.2057	0.0338	0.0	35.7207	24.9085	30.0323	0.0147
0.30	5°	0.03	1.1685	0.0448	0.0	26.0983	21.2103	24.7851	0.0103
0.30	5°	0.04	1.2590	0.0418	0.0	30.1135	21.9087	27.5830	0.0157
0.46	5°	0.03	1.2603	0.0564	0.0	22.3291	17.9936	22.6771	0.0136
0.46	5°	0.04	1.3640	0.0504	0.0	27.0848	19.9244	27.1764	0.0181

Table. 4 gives the CFJ performance with the variation of cruise Mach number. For the same C_μ, the CFJ total pressure ratio is increased by about 15% to 17% with the Mach number increased from 0.15 to 0.46. This is because that the wing flow energy loss is higher with the higher Mach number. The increased CFJ total pressure ratio is the main reason that the CFJ power coefficient is increased substantially in percentage as shown in Table. 3. The normalized CFJ mass flow rate per unit span is about the same with the different Mach number. The ratio of the jet velocity to freestream is also increased slightly for the same C_μ.

Table 4: Performance at different M_∞ for the 3D airplane with CFJ Wing at AR 20, AoA of 5° and C_μ of 0.03 and 0.04.

M_∞	AoA	C_μ	PR	P_{tinj}	$\dot{m}/span$	V_{inj}/V_∞
0.15	5°	0.03	1.0113	32.0600	0.1255	1.1841
0.15	5°	0.04	1.0158	32.2938	0.1463	1.3792
0.30	5°	0.03	1.0526	8.3149	0.1237	1.2055
0.30	5°	0.04	1.0689	8.5304	0.1440	1.4008
0.46	5°	0.03	1.1686	3.8697	0.1213	1.2283
0.46	5°	0.04	1.1939	4.1271	0.1414	1.4243

Table 5: Performance at different M_∞ for the 3D CFJ Wing at AR 20, AoA of 5° and C_μ of 0.03.

M_∞	AoA	C_μ	C_L	C_D	C_M	C_L/C_D	$(C_L/C_D)_c$	$({C_L}^2/C_D)_c$	P_c
0.15	5°	0.03	1.1829	0.0322	-0.1663	36.7375	29.0507	34.3646	0.0085
0.30	5°	0.03	1.2368	0.0338	-0.1732	36.5584	28.7406	35.5451	0.0092
0.46	5°	0.03	1.3156	0.0364	-0.1890	36.1788	27.5011	36.1794	0.0115

For comparison, Table 5 is the results with the wings only. The lift coefficient of the full aircraft is only slightly decreased from 1.7% to 4.4% compared with the wing only with the Mach number from 0.15 to 0.46. However, the C_L/C_D is decreased from 6.2% to 38%, and $(C_L/C_D)_c$ is decreased from 6.6% to 35%. This is because when the Mach number is increased, the flow separation occurs at the wing-fuselage conjunction. When C_μ is increased to 0.04 for the full aircraft, the C_L/C_D and $(C_L/C_D)_c$ are substantially improved by removing the flow separation at the wing-fuselage conjunction. At Mach number 0.46, the C_L/C_D and $(C_L/C_D)_c$ of the full aircraft is improved by 21.3% and 10.7% respectively. For the wing only, the overall aerodynamic performance does not vary much with the Mach number. But the full aircraft does vary significantly. The fuselage appears to be more suitable at the low Mach number of 0.15 than at a high Mach number of 0.46.

Fig. 7 is the Surface isentropic Mach number contours and streamlines at different cruise Mach number and C_μ of 0.03 and 0.04, and AoA of 5°. A minor flow separation at M_∞= 0.46 and C_μ = 0.03 in the area of the conjunction of the wing-fuselage is visible. At the lower flow Mach numbers, the flows are nicely attached.

(a) M_∞= 0.15 $C_\mu = 0.03$

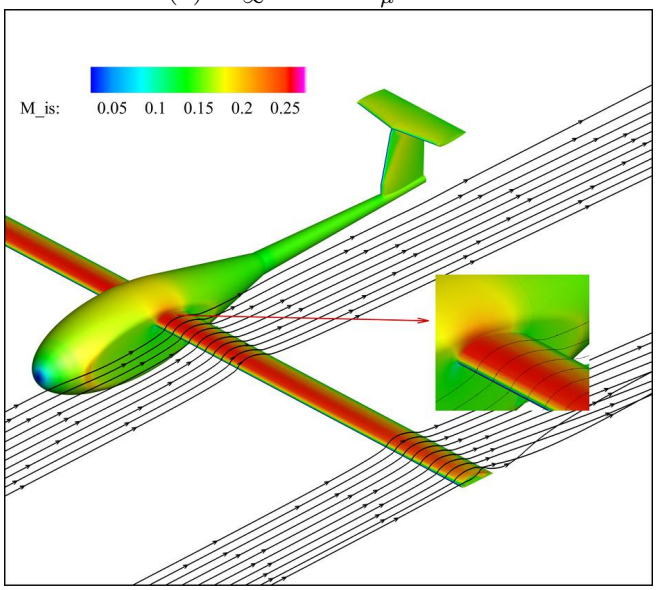

(b) $M_\infty = 0.15$ $C_\mu = 0.04$

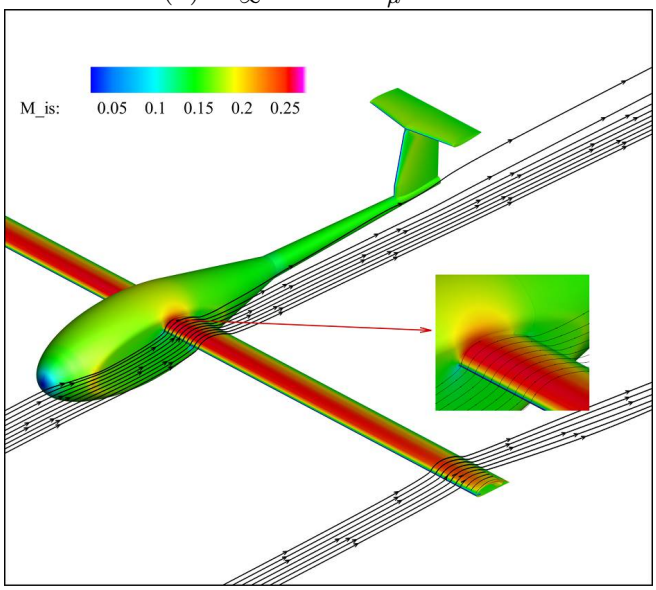

(c) $M_\infty = 0.30$ $C_\mu = 0.03$

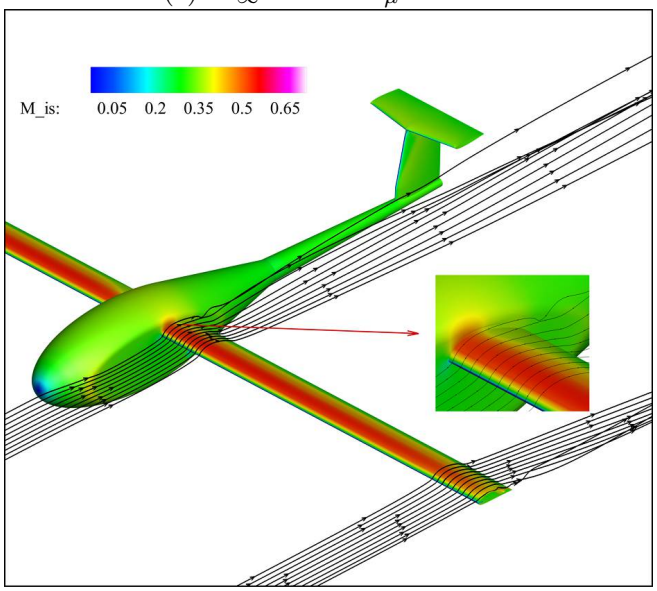

(d) M_∞= 0.30 $C_\mu = 0.04$

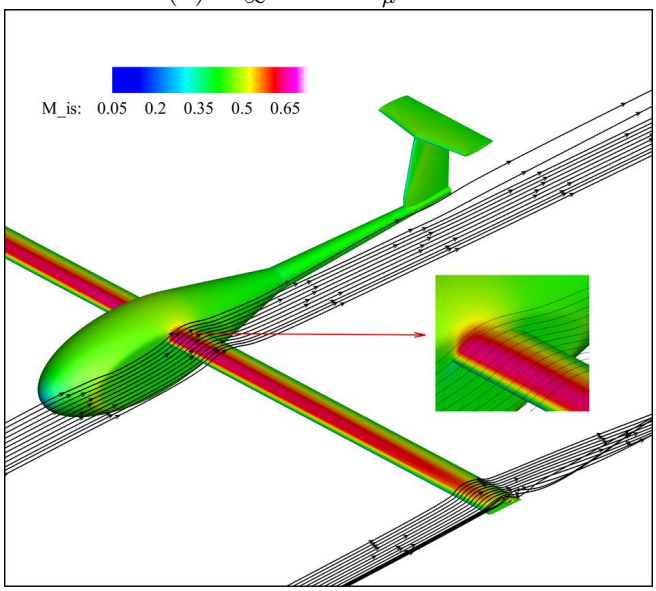

(e) M_∞= 0.46 C_μ = 0.03 (f) M_∞= 0.46 C_μ = 0.04

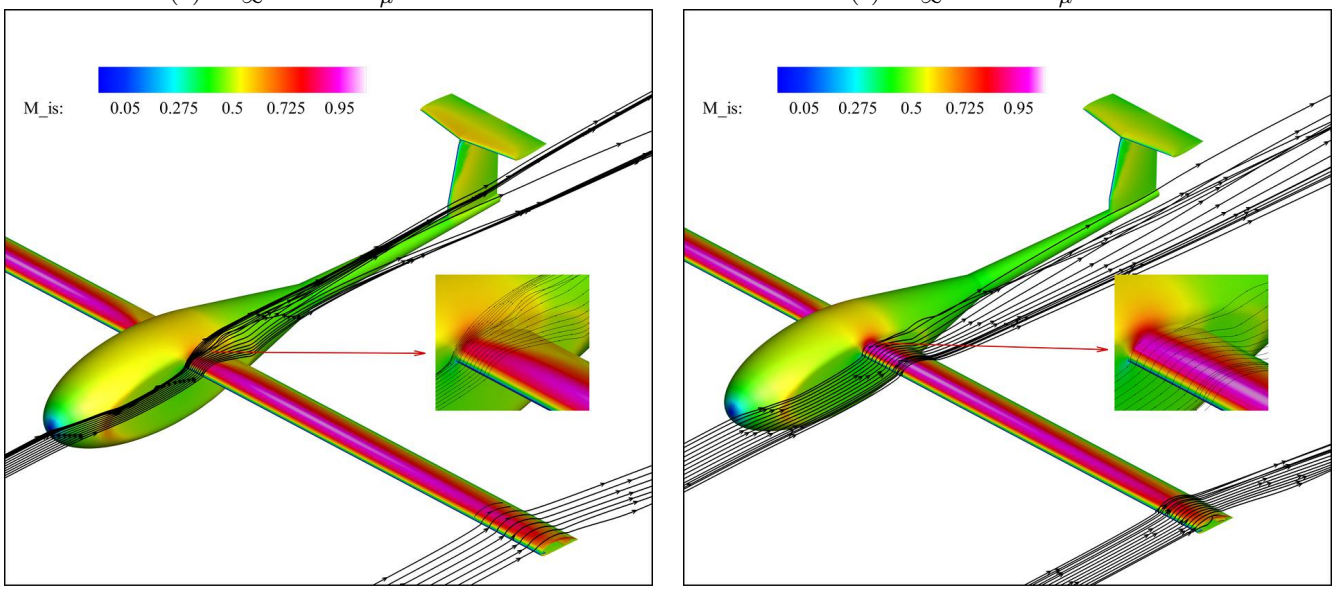

Figure 7: Surface isentropic Mach number contours and streamlines at different cruise Mach number and C_μ of 0.03 and 0.04, and AoA of 5°.

5 Conclusion

This paper numerically studies the Mach number effect on cruise performance of a Co-Flow Jet (CFJ) general aviation (GA) airplane at freestream Mach number of 0.15, 0.30, and 0.46 with an aspect ratio of 21.3. An optimized CFJ-NACA-6421 airfoil is used for the CFJ wing. The advantages of using a thick airfoil are two folds: 1) higher cruise lift coefficient; 2) lighter weight. The numerical simulations employ the intensively validated in house FASIP CFD code, which utilizes a 3D RANS solver with Spalart-Allmaras (S-A) turbulence model, 3rd order WENO scheme for the inviscid fluxes, and 2nd order central differencing for the viscous terms. Two constant C_μ of 0.03 and 0.04 are studied to examine the effect on the aircraft cruise performance. The angle of attack (AoA) is held at 5° corresponding to the optimal aerodynamic and productivity efficiency in the previous study for the wing performance at different Mach number. At C_μ of 0.03, the flow is very well attached for Mach 0.15, which gives the highest pure lift to drag ratio C_L/C_D, the corrected aerodynamic efficiency with CFJ power coefficient included $(C_L/C_D)_c$, and the productivity efficiency $(C_L^2/C_D)_c$. When the Mach number is increased to 0.46, the lift coefficient is increased by 8.6% from 1.16 to 1.26 due to the compressibility effect, but all the three aerodynamic performance parameters, C_L/C_D, $(C_L/C_D)_c$, and $(C_L^2/C_D)_c$ drop substantially. The reason is that the a flow separation at the wing-fuselage junction occurs. The drag coefficient is significantly increased by 67% when the Mach number is increased form 0.15 to 0.46 due to the flow separation, higher skin friction drag, and higher induced drag. When the C_μ is increased to 0.04, the wing-fuselage junction flow separation is removed. The CFJ power coefficient is increased by 33%, but remains at a very low level due to the low energy expenditure feature of the CFJ flow control. The C_L/C_D, $(C_L/C_D)_c$, and $(C_L^2/C_D)_c$ are significantly increased by 21.3%, 10.7%, and 19.8% respectively. In other words, the CFJ power increased due to C_μ of 0.04 at Mach 0.46 is converted to more system efficiency gain reflected by enhanced $(C_L/C_D)_c$ and $(C_L^2/C_D)_c$, which include the CFJ power coefficient. The system efficiency gains are attributed to the increased C_L and substantially reduced C_D due to the removed flow separation at low CFJ energy expenditure.

6 Acknowledgment

The simulations are conducted on Pegasus super computing system at the Center for Computational Sciences at the University of Miami.

Disclosure: The University of Miami and Dr. Gecheng Zha may receive royalties for future commercialization of the intellectual property used in this study. The University of Miami is also equity owner in CoFlow Jet, LLC, licensee of the intellectual property used in this study.

References

[1] G.-C. Zha and D. C. Paxton, "A Novel Flow Control Method for Airfoil Performance Enhancement Using Co-Flow Jet." *Applications of Circulation Control Technologies*, Chapter 10, p. 293-314, Vol. 214, Progress in Astronautics and Aeronautics, AIAA Book Series, Editors: Joslin, R. D. and Jones, G.S., 2006.

[2] G.-C. Zha, W. Gao, and C. Paxton, "Jet Effects on Co-Flow Jet Airfoil Performance," *AIAA Journal, No. 6,*, vol. 45, pp. 1222–1231, 2007.

[3] G.-C. Zha, C. Paxton, A. Conley, A. Wells, and B. Carroll, "Effect of Injection Slot Size on High Performance Co-Flow Jet Airfoil," *AIAA Journal of Aircraft*, vol. 43, 2006.

[4] G.-C. Zha, B. Carroll, C. Paxton, A. Conley, and A. Wells, "High Performance Airfoil with Co-Flow Jet Flow Control," *AIAA Journal*, vol. 45, 2007.

[5] Wang, B.-Y. and Haddoukessouni, B. and Levy, J. and Zha, G.-C., "Numerical Investigations of Injection Slot Size Effect on the Performance of Co-Flow Jet Airfoil," *Journal of Aircraft*, vol. Vol. 45, No. 6,, pp. pp.2084–2091, 2008.

[6] B. P. E. Dano, D. Kirk, and G.-C. Zha, "Experimental Investigation of Jet Mixing Mechanism of Co- Flow Jet Airfoil." AIAA-2010-4421, 5th AIAA Flow Control Conference, Chicago, IL, 28 Jun - 1 Jul 2010.

[7] B. P. E. Dano, G.-C. Zha, and M. Castillo, "Experimental Study of Co-Flow Jet Airfoil Performance Enhancement Using Micro Discreet Jets." AIAA Paper 2011-0941, 49th AIAA Aerospace Sciences Meeting, Orlando, FL, 4-7 January 2011.

[8] A. Lefebvre, B. Dano, W. Bartow, M. Fronzo, and G. Zha, "Performance and energy expenditure of coflow jet airfoil with variation of mach number," *Journal of Aircraft*, vol. 53, no. 6, pp. 1757–1767, 2016.

[9] A. Lefebvre, G-C. Zha, "Numerical Simulation of Pitching Airfoil Performance Enhancement Using Co-Flow Jet Flow Control," *AIAA paper 2013-2517*, June 2013.

[10] A. Lefebvre, G-C. Zha, "Cow-Flow Jet Airfoil Trade Study Part I : Energy Consumption and Aerodynamic Performance," *32nd AIAA Applied Aerodynamics Conference, AIAA AVIATION Forum, AIAA 2014-2682*, June 2014.

[11] A. Lefebvre, G-C. Zha, "Cow-Flow Jet Airfoil Trade Study Part II : Moment and Drag," *32nd AIAA Applied Aerodynamics Conference, AIAA AVIATION Forum, AIAA 2014-2683*, June 2014.

[12] Lefebvre, A. and Zha, G.-C., "Trade Study of 3D Co-Flow Jet Wing for Cruise Performance." AIAA Paper 2016-0570, AIAA SCITECH2016, AIAA Aerospace Science Meeting, San Diego, CA, 4-8 January 2016.

[13] Lefebvre, A. and Zha, G.-C. , "Design of High Wing Loading Compact Electric Airplane Utilizing Co-Flow Jet Flow Control." AIAA Paper 2015-0772, AIAA SciTech2015: 53nd Aerospace Sciences Meeting, Kissimmee, FL, 5-9 Jan 2015.

[14] Wang, Yang and Zha, G.-C., "Study of Mach Number Eect for 3D Co-Flow Jet Wings at Cruise Conditions." AIAA Paper 2020-0045, AIAA Scitech 2020 Forum , Orlando, FL, 6-10 January 2020.

[15] Yunchao Yang and Gecheng Zha, "Super-Lift Coefficient of Active Flow Control Airfoil: What is the Limit?." AIAA Paper 2017-1693, AIAA SCITECH2017, 55th AIAA Aerospace Science Meeting, Grapevine, January 9-13 2017.

[16] Wang, Yang and Zha, G.-C., "Study of Mach Number Effect for 2D Co-flow Jet Airfoil at Cruise Conditions." AIAA AVIATION Forum 2019, AIAA Aviation and Aeronautics Forum and Exposition, Dallas, Texas, June 17-21, 2019.

[17] Wang, Yang. and Yang, Yunchao. and Zha, G.-C., "Study of Super-Lift Coefficient of Co-Flow Jet Airfoil and Its Power Consumption." AIAA AVIATION Forum 2019, AIAA Aviation and Aeronautics Forum and Exposition, Dallas, Texas, June 17-21, 2019.

[18] Wang, Yang and Zha, G.-C., "Study of 3D Co-Flow Jet Wing Induced Drag and Power Consumption at Cruise Conditions." AIAA Paper 2019-0034, AIAA Scitech Forum 2019, San Diego, California, January 7-11, 2019.

[19] Lefebvre, A. and Dano, B. and Bartow, W. and Di Franzo, M. and Zha, G.-C., "Performance Enhancement and Energy Expenditure of Co-Flow Jet Airfoil with Variation of Mach Number." AIAA Paper 2013-0490, AIAA Journal of Aircraft, DOI: 10.2514/1.C033113, 2016.

[20] P. R. Spalart and S. R. Allmaras, "A one-equation turbulence model for aerodynamic flows," in *30th Aerospace Sciences Meeting and Exhibit, Aerospace Sciences Meetings, Reno, NV, USA, AIAA Paper 92-0439*, 1992.

[21] Y.-Q. Shen and G.-C Zha, "Large Eddy Simulation Using a New Set of Sixth Order Schemes for Compressible Viscous Terms ," *Journal of Computational Physics*, vol. 229, pp. 8296–8312, 2010.

[22] Zha, G.C., Shen, Y.Q. and Wang, B.Y., "An improved low diffusion E-CUSP upwind scheme ," *Journal of Computer and Fluids*, vol. 48, pp. 214–220, Sep. 2011.

[23] Y.-Q. Shen and G.-Z. Zha , "Generalized finite compact difference scheme for shock/complex flowfield interaction," *Journal of Computational Physics*, vol. doi:10.1016/j.jcp.2011.01.039, 2011.

[24] Shen, Y.-Q. and Zha, G.-C. and Wang, B.-Y., " Improvement of Stability and Accuracy of Implicit WENO Scheme," *AIAA Journal*, vol. 47, No. 2, pp. 331–344, 2009.

[25] Shen, Y.-Q. and Zha, G.-C. and Chen, X.-Y., " High Order Conservative Differencing for Viscous Terms and the Application to Vortex-Induced Vibration Flows," *Journal of Computational Physics*, vol. 228(2), pp. 8283–8300, 2009.

[26] Shen, Y.-Q. and Zha, G.-C. , " Improvement of the WENO Scheme Smoothness Estimator," *International Journal for Numerical Methods in Fluids*, vol. DOI:10.1002/fld.2186, 2009.

[27] G.-C. Zha and E. Bilgen, "Numerical Study of Three-Dimensional Transonic Flows Using Unfactored Upwind-Relaxation Sweeping Algorithm," *Journal of Computational Physics*, vol. 125, pp. 425–433, 1996.

[28] B.-Y. Wang and G.-C. Zha, "A General Sub-Domain Boundary Mapping Procedure For Structured Grid CFD Parallel Computation," *AIAA Journal of Aerospace Computing, Information, and Communication*, vol. 5, No.11, pp. 2084–2091, 2008.

[29] Y.-Q. Shen, G.-C. Zha, and B.-Y. Wang, "Improvement of Stability and Accuracy of Implicit WENO Scheme ," *AIAA Journal*, vol. 47, pp. 331–344, 2009.